Available online at www.sciencedirect.com
SCIENCE DIRECT
ELSEVIER
Journal of the European Ceramic Society 26 (2006) 2991–2997
ECERS
www.elsevier.com/locate/jeurceramsoc

Mixed conduction induced by grain boundary engineering

E. Gomes [a,c], F.M. Figueiredo [b,c], F.M.B. Marques [c,*]

[a] *ESTG, Instituto Politécnico de Viana do Castelo, P4900-348 Viana do Castelo, Portugal*
[b] *Science and Technology Department, Universidade Aberta, R. Escola Politécnica 147, P1269-001 Lisbon, Portugal*
[c] *Department of Ceramics and Glass Engineering, CICECO, University of Aveiro, P3810-193 Aveiro, Portugal*

Available online 15 March 2006

Abstract

Mixed oxygen-ion electronic conductors were prepared starting from the well-established solid electrolyte $La_{0.95}Sr_{0.05}Ga_{0.90}Mg_{0.10}O_{3-\delta}$ (LSGM). The adopted strategy involved selective grain boundary doping with iron to form a grain boundary region with high electronic conductivity. Scanning electron microscopy coupled with energy dispersive spectroscopy (SEM/EDS), impedance spectroscopy in air (around 300 °C) and high temperature (700–800 °C) ac conductivity measurements as a function of p_{O_2} all suggest that this doping strategy was successful. In fact, on increasing the Fe-dopant level, Fe always concentrated along the grain boundary region (as confirmed by SEM/EDS), the total conductivity increased and each individual impedance arc decreased, in agreement with predictions based on the presence of a parallel pathway for electronic transport. Furthermore, the increase in total conductivity (σ) with dopant level showed a positive $\log \sigma$ versus $\log p_{O_2}$ dependence, typical of hole conductivity.

Keywords: Lanthanum gallate; Ionic conductivity

1. Introduction

Mixed oxygen-ion electronic conductors have been known for many years but the envisaged applications were mostly as electrode materials for solid oxide fuel cells and similar electrochemical devices. The basic idea was that mixed conduction would favor delocalized electrochemical reactions occurring at the electrodes, with positive consequences in terms of lowering polarization losses.[1] Recent enthusiasm for permeating membranes, for methane partial oxidation reactors, justified an enhanced search for optimized mixed conductors.

Strategies to enhance mixed conduction starting from solid electrolytes included, predominantly, doping with mixed valence cations[2–9] and processing of composites with one dominant ionic and one dominant electronic conductor.[10–21] All these solutions proved to be of limited effectiveness. The levels of electronic conduction obtained by doping are usually modest while phase interaction and development of ion-blocking interfaces is almost unavoidable in the case of composites.

As an alternative to these strategies, the idea of heterogeneous microstructures is exploited in this work. Accordingly, starting from a well-known solid electrolyte, the possible formation of electronically conducting grain boundaries was addressed. A successful development of this kind of material should ensure that such grain boundaries are not ion-blocking and also that a percolation level is reached throughout the grain boundaries with this "heterogeneous" doping. Minimum disturbance of the bulk grain composition is envisaged to ensure preservation of high ionic conductivity.

Additional complex effects on the transport properties due to the presence of a new type of interface between the grain bulk and periphery may occur. For example, an enhancement in ionic conductivity was observed for core-shell $CaTiO_3$–$CaTi_{0.8}Fe_{0.2}O_{3-\delta}$ ceramics with respect to homogeneous $CaTi_{0.8}Fe_{0.2}O_{3-\delta}$.[22] This is probably due to new features created in the shell such as additional oxygen pathways induced by microdomain boundaries, space charge areas adjacent to the domain and/or the core–shell boundaries or even strain resulting from lattice mismatch between the core and the shell.

While the concept seems reasonably simple, selection of appropriate materials is not so easy and identification of ideal processing conditions is also time consuming. Previous work on several electrolytes and mixed conductors suggested the adoption of LSGM as a base material. The high ionic conductivity of this type of perovskite, discovered about 10 years ago, together with the tolerance of the perovskite structure to different types

* Corresponding author. Tel.: +351 234 370269; fax: +351 234 425300.
E-mail address: fmarques@cv.ua.pt (F.M.B. Marques).

0955-2219/$ – see front matter © 2006 Elsevier Ltd. All rights reserved.
doi:10.1016/j.jeurceramsoc.2006.02.017

of doping in the A- and B-sites,[23–30] suggested the possibility of smooth changes from isolated secondary phases along the grain boundaries to the formation of external layers within the grains, with progressive depletion of the foreign dopant while moving to the grain interior. Processing conditions, kinetic and thermodynamic parameters (e.g. diffusion via grain boundaries and the bulk, solubility of foreign dopants in the host lattice) are of major relevance in determining the final result.

Considering all these aspects and existing knowledge on these systems, Fe was selected as dopant to try to change the grain boundary performance of these materials while preserving the bulk behavior. Small amounts of Fe-additions to these perovskites are known to have even a moderate positive influence on the ionic conductivity of LSGM. Also, ferrites in general, are good electronic conductors that also possess significant ionic conductivity (e.g. $SrFeO_3$-based materials).[31,32] Furthermore, Fe diffusion via grain boundaries of LSGM is known to occur much faster than through the bulk, with orders of magnitude difference in the corresponding diffusion coefficients.[33]

Details of the experimental solution adopted and obtained results are presented in the following sections. However, the relevance of electronic transport properties on the dc and ac electrical performance of mixed conductors will firstly be addressed, to enhance the rationale of this strategy and introduce the expected performance of this type of materials.

2. Basic relations

The simplest description of a mixed conductor using a dc equivalent circuit can be found in Fig. 1.[34] This equivalent circuit shows two separate branches related to the ionic and electronic transport. The ideal cell open circuit voltage (V_o), due to the different oxygen potentials in contact with the cell surfaces, can be obtained from the Nernst law:

$$V_o = \left(\frac{RT}{4F}\right) \ln\left(\frac{p_{O_{2,I}}}{p_{O_{2,II}}}\right) \quad (1)$$

with R, T and F having their usual meanings, and $p_{O_{2,I}}$ and $p_{O_{2,II}}$ being the oxygen partial pressures (p_{O_2}) in contact with the cell surfaces. The cell effective voltage (V) might deviate significantly from the ideal value. Simple circuit analysis shows that:

$$V = V_o + I_o R_o \quad (2)$$

or

$$V = I_e R_e \quad (3)$$

where R_o and R_e are the ionic and electronic resistances of the cell, and I_o and I_e represent the ionic and electronic currents crossing the cell. Under open circuit conditions, I_o and I_e are equal in magnitude but opposite in sign and direction. This can be expressed as:

$$I_o + I_e = 0 \quad (4)$$

Eq. (4) simply states that, under open circuit conditions, there is no net charge flowing through the external circuit but two internal currents (partly) short circuit the cell. This ionic current is known as the electrochemical permeability of the mixed conductor.

In the present treatment, for the sake of simplicity, the ionic and electronic conductivities are assumed constant, irrespective of the oxygen activity, which allows for this simple description of the cell. For a more accurate analysis of the problem, the conductivity dependence on the oxygen partial pressure must be considered. This type of treatment can be found elsewhere.[35]

The combination of Eqs. (2)–(4) yields:

$$V = V_o \frac{R_e}{R_e + R_o} \quad (5)$$

and

$$I_o = \frac{V_o}{R_e + R_o} \quad (6)$$

Eq. (5) shows that V equals V_o when the electronic resistance becomes infinite; it is the case of a solid electrolyte. The smaller the value of R_e, the larger the deviation of V from V_o then the better mixed conducting properties. Eq. (6) shows that the current crossing the cell under open circuit depends mostly on R_e, as the ionic resistance is expected to be much smaller than the electronic one, if the starting material is a solid electrolyte, as considered in the present work. If the starting point is $R_o \ll R_e$, any abatement in electronic resistance will have a serious impact on the cell electrochemical permeability. Therefore, high electronic conductivity, either intrinsic or extrinsic (either "engineered" grain boundary or "core-shell" type microstructure), has positive consequences in terms of enhanced mixed conduction and oxygen permeability.

The simple dc equivalent circuit (Fig. 1A) comprising two parallel branches corresponding to the ionic and electronic transport is no longer valid when considering the ac response of such

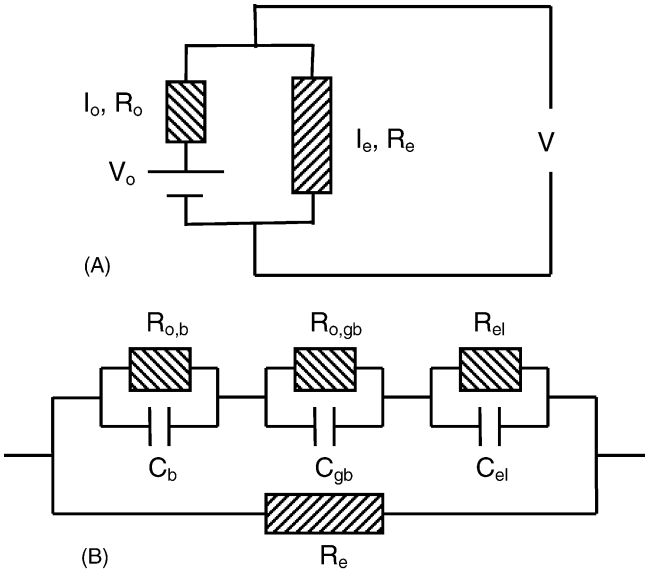

Fig. 1. Schematic description of a mixed conductor using: (A) one dc equivalent circuit; (B) one ac equivalent circuit. The meaning of all symbols can be found in the text.

cells. While the electronic branch usually can still be represented as a simple resistor, the ionic branch should include at least two resistance–capacitance (RC) elements, connected in series, related to the bulk and grain boundary contributions. This kind of description is the result of the so-called brick-layer model, which is, again, simplified but adequate in most cases. A more accurate description of actual materials, to take into account the common identification of depressed arcs in the usually called impedance spectra, should consider two RQ elements in series (instead of RC elements), with Q being a constant phase angle element.

The electrode response is by far more complex, requiring a variety of solutions depending on the exact cell under consideration. For the sake of simplicity, one additional RC circuit will be used for the present stage of discussion.

The impedance spectra corresponding to this type of simplified equivalent circuit with three RC elements (Fig. 1B) consists of three arcs, as shown in Fig. 2. The intermediate- and high-frequency intercepts of the real axis provide estimates for the grain-bulk and total (bulk + boundary) resistances of a solid electrolyte, $R_{o,b}$ and $R_{o,t}$. The grain boundary resistance, $R_{o,gb}$, can be obtained from the difference between total and bulk resistances.

Fig. 2A and B try to emphasize the role of the relative magnitude of a parallel electronic pathway on the cell impedance spectra. Fig. 2A includes a series of examples starting from a solid electrolyte where the bulk resistance is much larger than the grain boundary resistance. Fig. 2B addresses the opposite case. Obviously, increasing electronic conductivity of this ideal material leads to an apparent decrease in $R_{o,b}$ and $R_{o,t}$ values. The word apparent here should be emphasized as we are now looking at arcs which are the combined result of ionic and electronic resistances. In fact, the intercepts no longer represent the original ionic resistance, nor do they correspond to a simple relation between the original ionic and the total electronic contributions. In fact, the new intercepts include combined effects of all resistances present in the circuit. Furthermore, without a deeper knowledge of the exact changes faced by the ionic bulk and grain boundary resistances, attempts to estimate anything but the total electronic conductivity (even so, assuming preservation of the initial ionic contributions) are hardly sustainable. All these comments are required to emphasize that although we are able to predict a general trend for the impedance spectra of a given material, where heterogeneous doping might establish a parallel electronic pathway without disturbing the original ionic transport characteristics, without a deeper microstructural characterization and even exact determination of local transport properties (namely across grain boundaries, using microelectrodes if feasible), estimates of additional parameters from simple (comparative) analysis of impedance spectra has no real foundation.

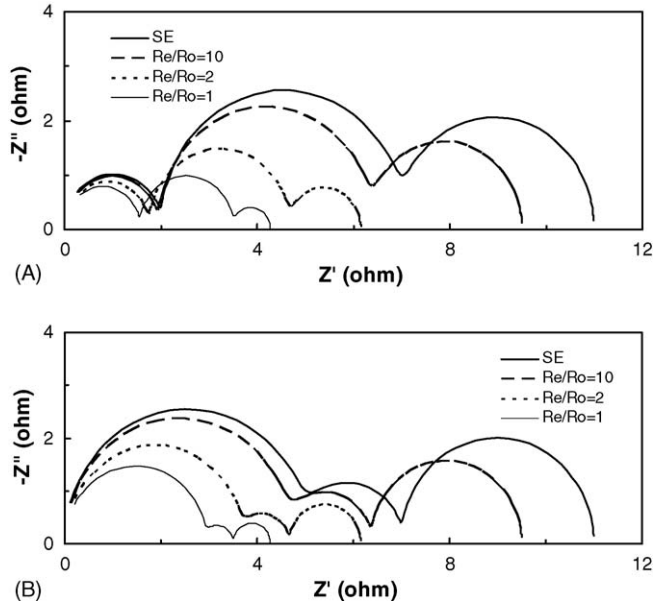

Fig. 2. Impedance spectra simulated for the circuit presented in Fig. 1B, for several values of R_e/R_o, where R_o is the total ionic conductivity: (A) dominant grain boundary resistance; (B) dominant bulk grain resistance. SE applies to solid electrolyte.

3. Experimental

Dense samples with nominal $La_{0.95}Sr_{0.05}Ga_{0.90}Mg_{0.10}O_{3-\delta}$ composition were prepared via the conventional ceramic route starting from high purity lanthanum (Merck), gallium (Aldrich) and magnesium (Panreac) oxides, and $SrCO_3$ (Merck). The precursors were mixed in ethanol in a planetary ball-mill, dried and calcined at 1100 °C for 12 h and again ball-milled and dried. The resultant powder was pressed into disk-shaped pellets and subsequently sintered at 1550 °C for 4 h with heating and cooling rates of 5 K/min. The X-ray diffraction (XRD) pattern, collected at room temperature from a powdered sample, could be indexed in the Pnma orthorhombic space group. A small amount of a secondary unidentified phase was suggested by a very small diffraction peak. Scanning electron microscopy combined with chemical analysis (SEM/EDS) confirmed the presence of a small number of Sr-enriched grains dispersed in the ceramic matrix. The grain size was found to vary in a broad range from about 5 to 15 μm. Finally, these samples have a density greater than 93% of the theoretical value (determined from XRD data).

The LSGM pellets, having both surfaces polished with 1 μm grained diamond paste, were sandwiched between two $LaFeO_{3-\delta}$ dense pellets and annealed in air at 1550 °C to promote the diffusion of Fe along the LSGM grain boundaries. The pellets were submitted to various annealing cycles of 1 h each. The heating and cooling rates were 5 K/min.

The electrical properties of the ceramic samples were studied by impedance spectroscopy in air between 300 and 500 °C. The spectra were collected in the frequency range 20–10^6 Hz with V_{ac} = 100 mV using a Hewlett Packard 4284A impedance analyser. Results were fitted to equivalent circuits using dedicated codes, either Equivalent Circuit (Version 3.97, 1989, B. Boukamp) or ZView (Version 2.6b, 1990–2002, Scribner Associates).

Fresh platinum electrodes were applied before every measurement and gently removed before the subsequent annealing. The same equipment was used to assess the oxygen partial

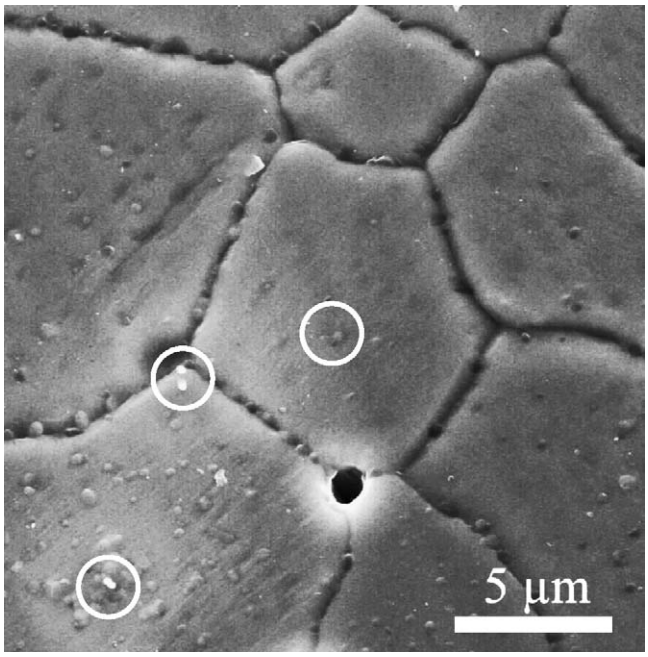

Fig. 3. SEM micrograph of Fe-doped LSGM after three impregnation cycles.

pressure (p_{O_2}) dependence of the total conductivity in order to identify the envisaged onset of p-type electronic conduction. These measurements were carried out at 700–750 °C and with p_{O_2} varying from air down to about 10 Pa, by flowing nitrogen + oxygen gas mixtures.

Several samples were specially prepared for SEM and EDS analyses following the normal procedure: polishing down to 0.25 μm diamond paste and by thermal etching at 1450 °C. Fractured, non-polished surfaces were also observed.

4. Results and discussion

4.1. Microstructure

The SEM microstructure shown in Fig. 3 was obtained for an LSGM pellet after three impregnation cycles at 1550 °C of 1 h each. The grain size remains nearly unchanged throughout the impregnation cycles and is fairly large (in the range 5–15 μm), as usually reported for LSGM ceramics obtained by the ceramic route and sintered at temperatures higher than 1500 °C. The white spots are the marks left by the electron beam during EDS analysis.

Typical EDS spectra collected at the centre and periphery of the grain are shown in Fig. 4. It can be seen that Fe is present only at the grain periphery. The analyses of several grains indicate that the thickness of the doped region is in the range 1–2 μm.

The observation of the pellet cross-section revealed that the Fe peaks were absent from the spectra obtained at about 100 μm away of each surface. However, the fact that the pellets were dark all over suggests that the impregnation was effective beyond the surfaces. It should be noticed that, given the geometric configuration of the LSGM/$LaFeO_3$ diffusion couple, an iron concentration gradient is expected to form from the outer surfaces to the bulk of the LSGM pellet.

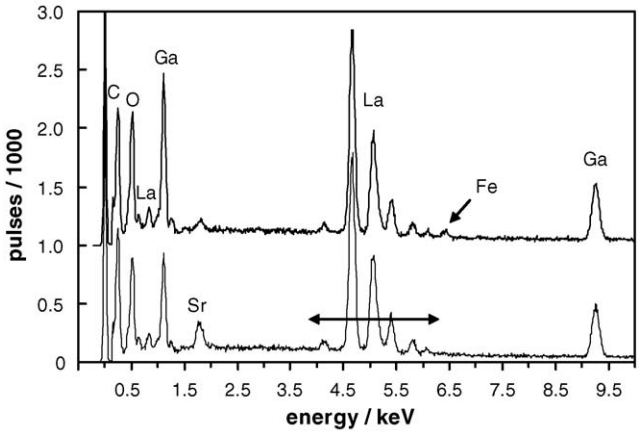

Fig. 4. EDS spectra collected at the spots showed in Fig. 3: bottom spectrum collected at the centre of the grain; top spectrum collected at the periphery, in which the Fe peak is apparent.

4.2. Impedance spectroscopy

The impedance spectra collected in air at 300 °C for the fresh LSGM and impregnated ceramics are shown in Fig. 5. The LSGM sample spectrum consists of high and low frequency contributions, usually ascribed to the bulk and grain boundary polarisations, respectively. The spectra were thus fitted to an equivalent circuit comprising two resistors in parallel with constant phase elements, for the reason previously discussed. In this circuit, represented as $(R_{o,b}Q_b)(R_{o,gb}Q_{gb})$, the subscripts b and gb denote bulk and grain boundary. The relevant fitting parameters are the bulk and grain boundary resistances ($R_{o,b}$, $R_{o,gb}$), the pseudocapacitances ($Q_{o,b}$, $Q_{o,gb}$) and the indexes that account for the depression of the semicircles (n_b, n_{gb}). The fitting results are listed in Table 1. The true capacitance values associated with each semicircle, determined by $C = R^{(1-n)/n}Q^{1/n}$, are 15 pF and 16 nF, respectively, for the high and low frequency contributions. The magnitude of these values is in close agreement with the expected ionic polarisation associated to grain and grain boundary contributions in a polycrystalline ionic conductor.

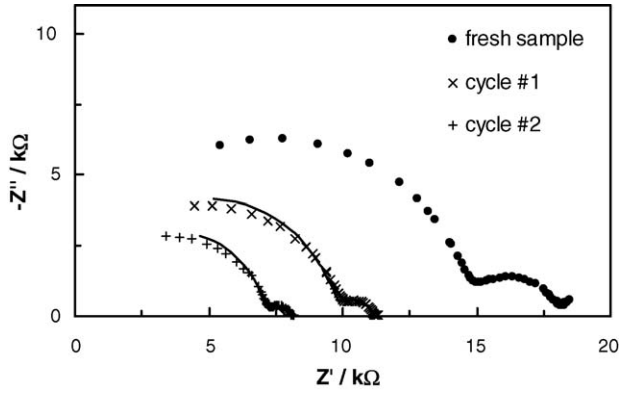

Fig. 5. Impedance spectra obtained in air at 300 °C for a fresh LSGM sample and after the first and second impregnation cycles. Lines are fits to the adopted equivalent circuit (see text for details).

Table 1
Fitting parameters obtained for fresh LSGM ceramics and used to obtain estimates of R_e for the impregnated samples

Parameter	Temperature (°C)			
	300	325	350	375
Grain bulk				
R_b (Ω)	14778	7187	3380	1711
$Q_b \times 10^{11}$	8.9	7.9	5.2	2.2
n_b	0.89	0.90	0.93	0.98
Grain boundary				
R_{gb} (Ω)	2810	1317	604	309
$Q_{gb} \times 10^8$	8.3	7.9	10.5	13.0
n_{gb}	0.84	0.85	0.82	0.81
R_e (Ω)[a]	13836	7121	3940	2546

Note: fitting errors are in the range 1–3% for R_i and n_i parameters and between 15 and 20% for Q_i.
[a] Fit of the cycle #2 spectra.

The effect of the impregnation with iron is apparent in the progressive decrease of the amplitude of both semicircles as the sample is submitted to an increasing number of impregnation cycles. Moreover, the effect is greater for the grain boundary contribution. Data obtained for several samples show that the trend is reproducible. This result strongly suggests that the overall increase in conductivity mainly results from the formation of a parallel electronic pathway with low resistance, as previously discussed.

In order to confirm that the nature of the additional charge carriers is electronic, the electrical conductivity of the samples was measured as function of p_{O_2} in moderately oxidising conditions. These results, presented in Fig. 6, show that the conductivity has a slight positive tendency with increasing p_{O_2}. Although almost negligible for the fresh sample, the inclination of the $\log \sigma$ versus $\log p_{O_2}$ slope is more pronounced for the Fe-impregnated samples. This means that the increase in conductivity should be due to an increase of the concentration of electron holes.

The samples microstructure and impedance spectroscopy results support a fairly simple model consisting of a bulk ionic conductor with grains surrounded by mixed ionic–electronic conducting grain boundaries. This corresponds to the equivalent circuit already presented while introducing Fig. 1B. This circuit was thus used to fit the spectra for the impregnated samples in order to obtain estimates of R_e while keeping the other parameters fixed and set equal to those of the fresh sample (Table 1). The lines in Fig. 5 reveal the best fit for the 300 °C spectra for one and two impregnation cycles. The quality of the fit is fairly good, considering that the model has one single variable. The resulting R_e values are given in Table 1 for several temperatures.

According to the present hypothesis, the R_e values could be used to obtain estimates of the p-type electronic conductivity by $\sigma_p = L/SR_e^{-1}$, where L and S are the length and cross section area geometric parameters defining the volume available for transport. Assuming the thickness L_p (0.146 cm) of the pellet and the surface area S_p (0.238 cm^2) of the platinum electrode, the value of σ_p after the second impregnation cycle is 1.76×10^{-5} S/cm. As mentioned above, these estimates, obtained by simple comparative analysis, lack real support mostly due to the uncertainty in the dopant distribution. A deeper knowledge of the microstructure or the determination of local transport properties (e.g. using micro-electrodes) are key issues for a more precise evaluation of the electrical properties of such heterogeneous materials. However, they still allow for some comparison with homogeneous $La_{0.9}Sr_{0.1}Ga_{1-x}Fe_xO_{3-\delta}$. As found for the latter compound, the electronic conductivity estimates obtained for the heterogeneous samples follows an Arrhenius-type behaviour with activation energy of about 75 kJ/mol (Fig. 7). This value, obtained at low temperature (300–375 °C), is lower than that obtained for the homogenous samples at 700–1000 °C, ca. 88.8 kJ/mol for $x = 0.2$ and 93.6 kJ/mol for $x = 0$.[36] Such a difference may be related to the fraction of tetravalent iron, which is expected to be higher at low temperature thus facilitating the hopping of small polarons between Fe^{4+} and Fe^{3+}, but also be representative of a highly

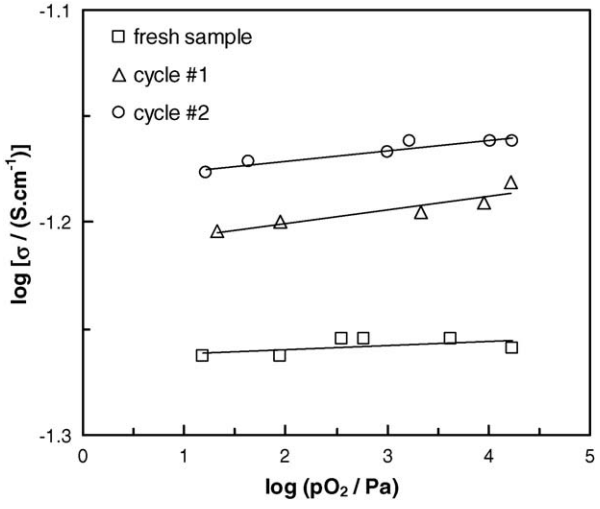

Fig. 6. Total electrical conductivity as a function of p_{O_2} at 750 °C for pure LSGM and Fe-impregnated samples.

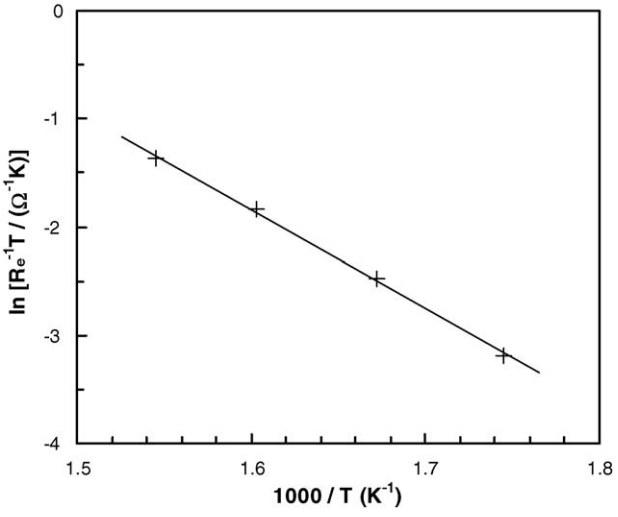

Fig. 7. Arrhenius representation of the electronic conduction parameter R_e in air for one Fe-doped LSGM sample after the second impregnation cycle.

localized concentration of Fe, probably in excess of the nominal compositions used for comparison.

5. Conclusions

Mixed conductors with one heterogeneous microstructure including grains with dominant ionic conduction and grain boundary regions with high electronic conductivity were prepared by localized grain boundary doping. The magnitude of the high frequency and intermediate frequency arcs observed in impedance spectra decreased with increasing amount of Fe along the grain boundaries, as predicted for the formation of a conductive electronic pathway. Also, the total conductivity showed a meaningful increasing dependence on oxygen partial pressure, typical of electron hole conduction. The potential of grain boundary engineering in developing new types of heterogeneous materials with enhanced performance was demonstrated. This route deserves further attention in order to overcome the constraints usually faced when dealing with common composite materials.

Acknowledgements

The authors express their gratitude for financial support from COST Action 525, PRODEP (E. Gomes) and FCT (Portugal), and CEC-Brussels (NoE FAME).

References

1. Schouler, E. J. L., Relations between solid oxide electrolyte surface-properties and electrode-reaction. *Solid State Ionics*, 1983, **9–10**, 945–951.
2. Steele, B. C. H., Powell, B. E. and Moody, P. M. R., Anionic conduction in refractory oxide solid solutions possessing the fluorite, pyrochlore and perovskite structures. *Proc. Br. Ceram. Soc.*, 1968, **10**, 87–102.
3. Cales, B. and Baumard, J. F., Conduction and defect structure of ZrO_2–CeO_2–Y_2O_3 solid solutions. *J. Electrochem. Soc.*, 1983, **131**, 2407–2413.
4. Liou, S. S. and Worrell, W. L., Electrical properties of novel mixed-conducting oxides. *J. Appl. Phys. A*, 1989, **49**, 25–31.
5. Liou, S. S. and Worrel, W. L., Mixed-conducting oxides electrodes for solid oxide fuel cells. In *Proceedings of the 1st International Symposium on Solid Oxide Fuel Cells*, ed. S. C. Singhal. The Electrochemical Society, Inc., Pennington, 1989, pp. 81–89.
6. Virkar, A. V., Nachlas, J., Joshi, A. V. and Diamond, J., Internal precipitation of molecular-oxygen and electrochemical failure of zirconia solid electrolytes. *J. Am. Ceram. Soc.*, 1990, **73**(11), 3382–3390.
7. Naito, H. and Arashi, H., Electrical properties of ZrO_2–TiO_2–Y_2O_3 system. *Solid State Ionics*, 1992, **53–56**, 436–441.
8. Lindegaard, T., Clausen, C. and Mogensen, M., Electrical and electrochemical properties of $Zr_{0.77}Y_{0.13}Ti_{0.1}O_{1.93}$. In *Proceedings of the 14th Riso International Symposium on Materials Science*, ed. F. W. Poulsen *et al.* Riso National Laboratory, Roskilde, 1993, pp. 311–318.
9. Marques, R. M. C., Marques, F. M. B. and Frade, J. R., Characterization of mixed conductors by DC techniques. Part II: Experimental results. *Solid State Ionics*, 1994, **73**, 27–34.
10. Shen, Y., Joshi, A., Liu, M. and Krist, K., Structure, microstucture and transport properties of mixed ionic–electronic conductors based on bismuth oxide. Part I. Bi–Y–Cu–O system. *Solid State Ionics*, 1994, **72**, 209–217.
11. Chen, C. S., Boukamp, B. A., Bouwmeester, H. J. M., Cao, G. Z., Kruidhof, H., Winnubst, A. J. A. *et al.*, Microstructural development, electrical properties and oxygen permeation of zirconia–palladium composites. *Solid State Ionics*, 1995, **76**, 23–28.
12. ten Elshof, J. E., Nguyen, N. Q., den Otter, M. W. and Bouwmeester, H. J. M., Oxygen permeation properties of dense $Bi_{1.5}Er_{0.5}O_3$–Ag cermet membranes. *J. Electrochem. Soc.*, 1997, **144**(12), 4361–4366.
13. Chen, C. S. and Burggraaf, A. J., Stabilized bismuth oxide–noble metal mixed conducting composites as high temperature oxygen separation membranes. *J. Appl. Electrochem.*, 1999, **29**, 355–360.
14. Park, Y. M. and Choi, G. M., Mixed ionic and electronic conduction in YSZ–NiO composite. *J. Electrochem. Soc.*, 1999, **146**(3), 883–889.
15. Kharton, V. V., Kovalevsky, A. V., Viskup, A. P., Figueiredo, F. M., Yaremchenko, A. A., Naumovich, E. N. *et al.*, Oxygen permeability of $Ce_{0.8}Gd_{0.2}O_{2-\delta}$–$La_{0.7}Sr_{0.3}MnO_{3-\delta}$ composite membranes. *J. Electrochem. Soc.*, 2000, **147**(7), 2814–2821.
16. Kim, J. and Lin, Y. S., Synthesis and oxygen permeation properties of ceramic-metal dual-phase membranes. *J. Membr. Sci.*, 2000, **167**, 123–133.
17. Kharton, V. V., Kovalevsky, A. V., Viskup, A. P., Figueiredo, F. M., Yaremchenko, A. A., Naumovich, E. N. *et al.*, Oxygen permeability and faradaic efficiency of $Ce_{0.8}Gd_{0.2}O_{2-\delta}$–$La_{0.7}Sr_{0.3}MnO_{3-\delta}$ composites. *J. Eur. Ceram. Soc.*, 2001, **21**, 1763–1767.
18. Wu, K., Xie, S., Jiang, G. S., Liu, W. and Chen, C. S., Oxygen permeation through $(Bi_2O_3)_{0.74}(SrO)_{0.26}$–Ag (40% v/o) composite. *J. Membr. Sci.*, 2001, **188**, 189–193.
19. Nigge, U., Wiemhofer, H.-D., Romer, E. W. J., Bouwmeester, H. J. M. and Schulte, T. R., Composites of $Ce_{0.8}Gd_{0.2}O_{1.9}$ and $Gd_{0.7}Ca_{0.3}CoO_{3-\delta}$ as oxygen permeable membranes for exhaust gas sensors. *Solid State Ionics*, 2002, **146**, 163–174.
20. Wang, H., Yang, W. S., Cong, Y., Zhu, X. and Lin, Y. S., Structure and oxygen permeability of a dual-phase membrane. *J. Membr. Sci.*, 2003, **224**, 107–115.
21. Kharton, V. V., Kovalevsky, A. V., Viskup, A. P., Shaula, A. L., Figueiredo, F. M., Naumovich, E. N. *et al.*, Oxygen transport in $Ce_{0.8}Gd_{0.2}O_{2-\delta}$-based composite membranes. *Solid State Ionics*, 2003, **160**, 247–258.
22. Figueiredo, F. M., Kharton, V. V., Waerenborgh, J. C., Viskup, A. P., Naumovich, E. N. and Frade, J. R., Influence of microstructure on the electrical properties of iron-substituted calcium titanate ceramics. *J. Am. Ceram. Soc.*, 2004, **87**(12), 2252–2261.
23. Ishihara, T., Matsuda, H. and Takita, Y., Doped $LaGaO_3$ perovskite type oxide as a new oxide ionic conductor. *J. Am. Chem. Soc.*, 1994, **116**, 3801–3803.
24. Feng, M. and Goodenough, J. B., A superior oxide-ion electrolyte. *Eur. J. Solid State Inorg. Chem.*, 1994, **31**, 663–672.
25. Huang, P. and Petric, A., Superior oxygen ion conductivity of lanthanum gallate doped with strontium and magnesium. *J. Electrochem. Soc.*, 1996, **143**, 1644–1648.
26. Stevenson, J. W., Armstrong, T. R., McGready, D. E., Pederson, L. R. and Weber, W. J., Processing and electrical properties of alkaline earth-doped lanthanum gallate. *J. Electrochem. Soc.*, 1997, **144**, 3613–3620.
27. Drennan, J., Zelizko, V., Hay, D., Ciacci, F. T., Rajendran, S. and Badwal, S. P., Characterisation, conductivity and mechanical properties of the oxygen-ion conductor $La_{0.9}Sr_{0.1}Ga_{0.8}Mg_{0.2}O_{3-x}$. *J. Mater. Chem.*, 1997, **7**, 79–83.
28. Baker, R. T., Gharbage, B. and Marques, F. M. B., Ionic and electronic conduction in Fe and Cr doped $(La,Sr)GaO_{3-\delta}$. *J. Electrochem. Soc.*, 1997, **144**, 3130–3135.
29. Kharton, V. V., Viskup, A. P., Naumovich, E. N. and Lapchuk, N. M., Mixed electronic and ionic conductivity of $LaCo(M)O_3$ (M = Ga, Cr, Fe or Ni): I. Oxygen transport in perovskites $LaCoO_3$–$LaGaO_3$. *Solid State Ionics*, 1997, **104**, 67–78.
30. Ishihara, T., Higuchi, M., Furutani, H., Fukushima, T., Nishiguchi, H. and Takita, Y., Potentiometric oxygen sensor operable in low temperature by applying $LaGaO_3$-based oxide for electrolyte. *J. Electrochem. Soc.*, 1997, **144**, L122–L125.
31. Yaremchenko, A. A., Patrakeev, M. V., Kharton, V. V., Marques, F. M. B., Leonidov, I. A. and Kozhevnikov, V. L., Oxygen ionic and electronic

conductivity of $La_{0.3}Sr_{0.7}Fe(Al)O_{3-\delta}$ perovskites. *Solid State Sci.*, 2004, **6**, 357–366.

32. Kharton, V. V., Shaulo, A. L., Viskup, A. P., Avdeev, M. Yu., Yaremchenko, A. A., Patrakeev, M. V. *et al.*, Perovskite-like system (Sr,La)(Fe,Ga)$O_{3-\delta}$: structure and ionic transport under oxidizing conditions. *Solid State Ionics*, 2002, **150**, 229–243.
33. Schulz, O. and Martin, M., Preparation and characterisation of $La_{1-x}Sr_xGa_{1-y}Mg_yO_{3-(x+y)/2}$ for the investigation of cation diffusion processes. *Solid State Ionics*, 2000, **135**, 549–555.
34. Patterson, J. W., Ionic and electronic conduction in nonmetallic phases, *ACS Symp. Series* (No. 89), Corrosion Chemistry, ed. G. Brubaker and P. Phipps. Am. Chem. Soc., Washington, DC, 1979, pp. 96–125.
35. Marques, R. M. C., Marques, F. M. B. and Frade, J. R., Characterization of mixed conductors by DC techniques. Part I: Theoretical solutions. *Solid State Ionics*, 1994, **73**, 15–25.
36. Gharbage, B., Figueiredo, F. M., Baker, R. T. and Marques, F. M. B., Electrochemical permeability of $La_{0.9}Sr_{0.1}Ga_{1-x}Fe_xO_{3-\delta}$. *Electrochim. Acta*, 2000, **45**, 2095–2099.